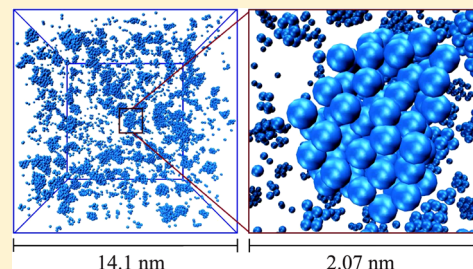


Steady-State Homogeneous Nucleation and Growth of Water Droplets: Extended Numerical Treatment

Anatolii V. Mokshin* and Bulat N. Galimzyanov

Department of Physics, Kazan Federal University, Kazan, Russia

ABSTRACT: The steady-state homogeneous vapor-to-liquid nucleation and the succeeding liquid droplet growth process are studied for water systems by means of the coarse-grained molecular dynamics simulations with the mW model suggested originally by Molinero et al. [Molinero, V.; Moore, E. B. *J. Phys. Chem. B* **2009**, *113*, 4008–4016]. The investigation covers the temperature range $273 \leq T/K \leq 363$ and the system's pressure $p \approx 1$ atm. The thermodynamic integration scheme and the extended mean first passage time method as tools to find the nucleation and cluster growth characteristics are applied. The surface tension is numerically estimated and is compared with the experimental data for the considered temperature range. We extract the nucleation characteristics such as the steady-state nucleation rate, the critical cluster size, the nucleation barrier, and the Zeldovich factor and perform the comparison with the other simulation results and test the treatment of the simulation results within the classical nucleation theory. We found that the liquid droplet growth is unsteady and follows the power law. Also, the growth laws exhibit the features unified for all of the considered temperatures. The geometry of the nucleated droplets is also studied.



INTRODUCTION

Nucleation is a fundamental process that characterizes the mechanisms of the emergence of a new phase, and this is one of the most widespread ways by which phase transitions are initiated. Although a variety of theoretical descriptions for the nucleation exists, all of them are based on the same key idea: a new phase starts to evolve within a mother phase from the nuclei, when they achieve such sizes and shapes, which facilitate the further stable growth of these nuclei. According to classical nucleation theory (CNT), the stability of the nuclei results from the confrontation of surface and bulk contributions in a free energy. This is relevant for the homogeneous scenario, which implies the equal probability of the appearance of a nucleation event over the sample, as well as for the heterogeneous scenario, where some places in a sample are more attractive for nucleation events (due to impurities, walls, etc.).

Concerning the specific case of the homogeneous droplet nucleation during the vapor-to-liquid transition in water, there is the comprehensive experimental material from a series of investigations (see, for example refs 1–9 and references therein). Here, a direct comparison of the experimental results with the predictions of the nucleation theories as well as with the data of the numerical simulations performed by means of molecular dynamics (MD)^{10,11} and Monte Carlo^{12,13} methods has revealed noticeable discrepancies. So, for example, for the vapor-to-liquid nucleation in water at identical conditions (pressure/supersaturation, temperature) the experiments, the theoretical models (CNT and others), and the numerical simulations yield values of the steady-state nucleation rate J_s , which differ by orders of magnitude. Under these circumstances, it could be quite reasonable to consider the features of

the nucleation–growth kinetics in water at the molecular level, treating the vapor-to-liquid transition in the context of molecular interactions and movements.

Recently, Molinero and Moore have suggested a coarse-grained “monatomic” model of water (mW), in which the anisotropy in the molecular interactions is simply realized by means of an angular-dependent contribution.¹⁴ The removal of the atomic interactions from consideration accelerates the computations, and thereby, it inspires the microscopic properties of the system to be probed on extended time scales. Here, the phase transitions are convenient candidates to be taken in handling. So, the homogeneous nucleation of ice was studied within the mW model of water in refs 15 and 16. Therefore, it is tempting to extend these studies and to consider the details of the vapor-to-liquid phase transition on the basis of the mW model. An important point is that the mW model reproduces correctly the equation of state for the temperature range $250 < T/K < 350$ at $p \approx 1$ atm. (see Figure 4 in ref 14), which is relevant to the consideration of the droplet nucleation in water.

From the viewpoint of CNT, three principal parameters are enough to restore the basic aspects of the steady-state nucleation. These can be, for example, the steady-state nucleation rate J_s , the nucleation barrier ΔG , and the Zeldovich factor Z . Of course, those three parameters can be taken in another combination (for example, the “reduced moment”, the lag-time, and the steady-state nucleation rate, like it is suggested in ref 17). Nevertheless, the surface tension σ , which

Received: May 18, 2012

Revised: September 1, 2012

Published: September 7, 2012

characterizes the interphase layer and contributes to the nucleation barrier through the surface free energy term, requires independent treatment.¹⁸ In the direct computer simulations, the different adapted convenient approaches based on the Fowler formula, the Kirkwood–Buff formula, and others are utilized to define accurately the surface tension.^{19,20} However, there is a necessity for the study of nucleation to apply such a method (i) that gives a possibility to estimate the surface tension from the raw simulation data, (ii) that is applicable to characterize the surfaces of the microscopical nuclei with a pronounced inherent curvature, and (iii) that considers the genuine interphase (vapor–liquid) properties without reference to a vacuum phase.

In the present work, we study the nucleation–growth processes of water droplets on the basis of MD simulations with the mW model. To define the parameters of the nucleation and the droplet growth, we apply a statistical treatment of the simulation data on the basis of the thermodynamic integration scheme and the mean first passage time (MFPT) approach. Similar to the thermodynamic integration scheme, the MFPT approach utilizes the time-dependent configurations from the independent runs under identical conditions; however, the MFPT is focused on the averaged time scales, at which a system characteristic (reaction coordinate, order parameter) appears for the first time.^{21–23} We show that the thermodynamic integration scheme and the MFPT method provide a convenient tool to treat the simulation results (and/or the experimental data) concerning both the nucleation and the growth kinetics. For the considered case of water, we define the set of characteristics for steady-state homogeneous nucleation and growth of the liquid droplets on the basis of MD simulation data.

NUMERICAL SCHEMES

Thermodynamic Integration. The surface energy w can be defined as an excess energy per unit area of the surface that is conditioned by the lack of neighbors for the surface particles in comparison with the bulk particles (see ref 24). If one restricts the consideration by the closest neighbors only with the pairwise additive interactions $u(r_{ij})$, then the following relation appears directly

$$w = \frac{1}{2} u(\hat{r}_{ij})(z - z')n' \quad (1)$$

where \hat{r}_{ij} is the average distance between the neighbors in a new phase, the quantity n' denotes the number of surface particles per unit area and depends on the size of a nucleus, and z and z' are the first coordination number of bulk and surface particles, respectively. Then, the surface tension can be estimated directly by the thermodynamic integration of the surface energy as

$$\sigma = - \int_{\lambda=0}^1 \left\langle \frac{\partial w}{\partial \lambda} \right\rangle_{\lambda} d\lambda \quad (2)$$

The reaction coordinate λ or the so-called λ -scaling²⁵ is associated with the rescaled cluster size, $\lambda = (n/n^*)^{1/3}$, which is equal to zero if there are no nuclei in the system and to unity if the nucleus size has the critical value n^* . The notation $\langle \dots \rangle_{\lambda}$ means an ensemble average at a particular value of λ .

Extended Mean First Passage Time Method. According to the continuous Zeldovich–Frenkel scheme, the nucleation process can be described within a Fokker–Planck-type equation

$$\frac{\partial N_n(t)}{\partial t} = -\frac{\partial J_n}{\partial n} = \frac{\partial}{\partial n} \left\{ N_n^{\text{eq}} g_n^+ \frac{\partial}{\partial n} \left[\frac{N_n(t)}{N_n^{\text{eq}}} \right] \right\} \quad (3)$$

where n is the cluster size, $N_n(t)$ is the time-dependent cluster size distribution over unit volume, J_n is the current over cluster size space, g_n^+ is the monomer attachment rate to a n -sized cluster, $N_n^{\text{eq}} = N_0^{\text{eq}} \exp(-\beta \Delta G_n)$ is the equilibrium cluster size distribution, ΔG_n is the work required to form the n -sized cluster, and $\beta = 1/(k_B T)$.

If one considers the n -dependent term ΔG_n , the nucleation regime is directly associated with the vicinity of the critical value of the cluster size, n^* , where the term ΔG_{n^*} corresponds to a nucleation barrier and has a maximum. Assuming that the nucleation barrier can be expanded into the Taylor series in this vicinity

$$\Delta G_n = \Delta G_{n^*} + \sum_{k=2} \frac{(n - n^*)^k}{k!} \frac{\partial^k \Delta G_n}{\partial n^k} \bigg|_{n=n^*} \quad (4)$$

the approximated evaluation of eq 3 in the vicinity of the nucleation regime can be written as

$$J_{n'}^{-1} = \frac{\exp(\beta \Delta G_{n^*})}{g_{n^*}^+ N_0^{\text{eq}}} \int_0^{n'} dn \exp \left[\beta \sum_{k=2} \frac{(n - n^*)^k}{k!} \frac{\partial^k \Delta G_n}{\partial n^k} \bigg|_{n=n^*} \right] \quad (5)$$

The series in the exponential of eq 5 contains information about the geometrical peculiarities of the term ΔG_n around its maximum at n^* . Namely, the second contribution of the series is related with the Zeldovich factor Z and characterizes the curvature of the barrier at the top

$$-\frac{\beta}{2} \frac{\partial^2 \Delta G_n}{\partial n^2} \bigg|_{n=n^*} = \pi Z^2 \quad (6)$$

Moreover, the ratio of the third and the second contributions, which is $\Delta G_{n=n^*}^{(3)}/3\Delta G_{n=n^*}^{(2)}$, indicates on the asymmetric properties of the barrier. For example, if the ratio is equal to zero, then the barrier is symmetric and can be approximated by a parabolic geometry. This means for the given example that we are restricted here only by a case with $k = 2$, which corresponds to the Zeldovich approximation. Here, the analytical expression for the steady-state nucleation rate J_s can be directly obtained from eq 5 within the MFPT method,²⁶ where the averaged time scale of the first appearance of the n -sized cluster τ_n^{MFPT} is considered:

$$\begin{aligned} \tau_n^{\text{MFPT}} &= \frac{1}{2J_s V} \{1 + \text{erf}[\sqrt{\pi} Z(n - n^*)]\} \\ &= \frac{1}{2J_s V} \text{erfc}[\sqrt{\pi} Z(n - n^*)] \end{aligned} \quad (7)$$

Here V is the system volume and $\text{erf}(x) = 2\pi^{-1/2} \int_0^x \exp(-t^2) dt$ is the error function.

The MFPT method provides the next useful capabilities in the treatment of the nucleation–growth processes. The first one is related with the critical value n^* , which is located at the inflection point, i.e. at the point, where the first derivative $(\partial \tau_n^{\text{MFPT}} / \partial n)_{n=n^*}$ has a maximum. Thus, a simple analysis of $\partial \tau_n^{\text{MFPT}} / \partial n$ yields the critical value n^* (see Figure 1). For the

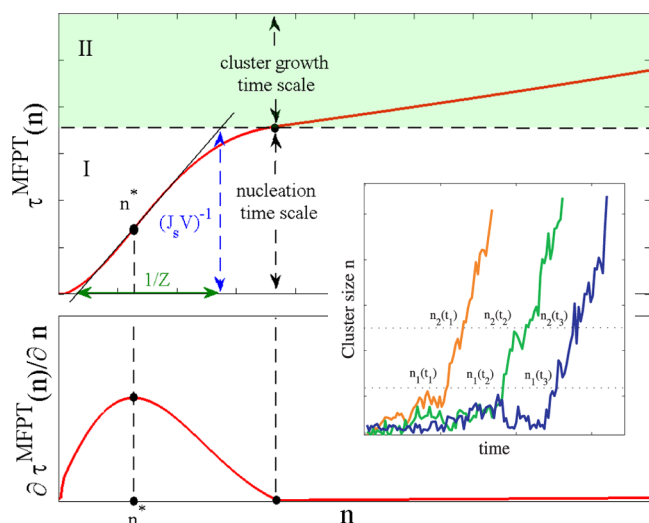


Figure 1. Top: Schematic plot of the MFPT distribution for the cluster size n as obtained from simulation (or experimental) data. The regions I and II are associated with nucleation and cluster-growth regimes, respectively. The routine for finding the nucleation characteristics from the MFPT curve is presented. The gentle slope of the MFPT curve at the transition value, $n = n^*$, is evidence of the smooth form of the nucleation barrier ΔG_n in the vicinity of n^* , whereas the location of the inflection point (full circle) below the half-height $1/(2J_s V)$ indicates qualitatively on the barrier asymmetry. The pronounced increase of the MFPT curve in region II appears due to the fact that nucleation and cluster-growth time scales are comparable, and this part of the curve as an inverted one, $n(\tau^{\text{MFPT}})$, can be used to estimate the parameters of cluster growth kinetics. Bottom: First derivative of the MFPT distribution, $\partial \tau_n^{\text{MFPT}} / \partial n$. Here, the maximum is associated with the inflection point, which is directly located at the critical value of cluster size, $n = n^*$. Position of the next extremum (minimum) on $(\partial \tau_n^{\text{MFPT}} / \partial n)_{n > n^*}$ corresponds to the nucleation time scale $\tau_n = 1/(2J_s V)$ as defined from the main MFPT distribution τ_n^{MFPT} . Inset: Typical cluster growth curves obtained from the independent simulations.

particular case of eq 7, one obtains directly that $n = n^*$, when $\tau_{n=n^*}^{\text{MFPT}} = 1/(2J_s V)$ that is the consequence of the nucleation barrier symmetry. The second property is that the Zeldovich factor can be directly extracted from MFPT as

$$Z = J_s V \left. \frac{\partial \tau_n^{\text{MFPT}}}{\partial n} \right|_{n=n^*} \quad (8)$$

The geometric constructions, corresponding to this equation, are presented in Figure 1. Equation 8 indicates that the smaller values of Z result from the smaller values of $(\partial \tau_n^{\text{MFPT}} / \partial n)_{n=n^*}$ at the fixed $J_s V$. On the other hand, the smaller values of the Zeldovich factor correspond to the flatter nucleation barrier curve ΔG_n near the critical size n^* . And, finally, the third property is associated with the steady-state nucleation rate J_s , which can be defined from the MFPT distribution as $J_s = 1/(\tau_n^{\text{MFPT}} V)$ at n , where $(\partial \tau_n^{\text{MFPT}} / \partial n)_{n > n^*}$ approaches the minimum and the distribution τ_n^{MFPT} starts itself to demonstrate a steady-like n -dependence (see Figure 1). Thus, using the known mean first passage time distribution τ_n^{MFPT} one can directly define the critical value n^* , the Zeldovich factor Z , and the steady-state nucleation rate J_s by a direct numerical analysis.

Nucleation–growth kinetics is characterized by the nucleation time scale $\tau_n = 1/(J_s V)$ and the cluster-growth time scale τ_{gr} . The ratio between these time scales distinguishes the

separate cases for the numerical treatment within the MFPT method: (i) if $\tau_n \gg \tau_{gr}$, then τ_n^{MFPT} demonstrates a clear defined plateau of the height $\tau_n = 1/(J_s V)$, that simplifies significantly accurate estimation of the nucleation rate; (ii) if these time scales are comparable, $\tau_n \approx \tau_{gr}$, then the errors can appear in the estimation of τ_n since the boundary between nucleation and growth in MFPT distribution is smeared.

Furthermore, the MFPT method gives a convenient tool to extract the characteristics of nucleus growth kinetics, which follows the nucleation regime in the MFPT distribution (see Figure 1). In fact, the inverted MFPT distribution, $n(\tau^{\text{MFPT}})$, has the statistical meaning of the most probable cluster growth law for the growth regime of the MFPT curve.

Following ref 27, the growth law of a cluster can be taken in general form as

$$R(t) = R_* + (\mathcal{G}_{cl} t)^\nu \quad (9)$$

where R and R_* is the radius of the growing cluster and the critically sized cluster, respectively; ν is the growth exponent and \mathcal{G}_{cl} is the growth constant, which has a dimension of $[m^{1/\nu}/s]$. Then, the growth rate is $G(t) = \nu \mathcal{G}_{cl}^\nu t^{\nu-1}$, while the acceleration of a cluster growth can be formally defined as $a(t) = \nu(\nu - 1) \mathcal{G}_{cl}^\nu t^{\nu-2}$. The steady cluster growth with a constant growth rate corresponds to the particular case of $\nu = 1$, where the growth rate coincides with the growth factor, i.e., $G(t) = \mathcal{G}_{cl} = \text{const}$, otherwise (at $\nu \neq 1$) one has the process with unsteady growth rate.²⁸ Further, taking into account that the volume of a growing cluster evolves with time as $V(t) = c_g [R(t)]^3$ and $N(t) = \rho_{cl} V(t)$, where c_g is a dimensionless cluster-shape factor ($c_g = 4\pi/3$ in a case of the sphere) and ρ_{cl} is the density of the cluster-phase, one can write the growth law in the extended form

$$n(t, t_c) = n^* \left[1 + \mathcal{G}_{cl}^{3\nu} (t - t_c)^{3\nu} \frac{\rho_{cl} c_g}{n^*} + 3 \mathcal{G}_{cl}^{2\nu} (t - t_c)^{2\nu} \left(\frac{\rho_{cl} c_g}{n^*} \right)^{2/3} + 3 \mathcal{G}_{cl}^\nu (t - t_c)^\nu \left(\frac{\rho_{cl} c_g}{n^*} \right)^{1/3} \right] \quad (10)$$

Here, the lag-time t_c defines the appearance of the critically sized cluster. Then, the term $n(\tau^{\text{MFPT}})$ can be fitted by eq 10 to extract the growth characteristics: the cluster-shape factor c_g , the growth constant \mathcal{G}_{cl} and the growth exponent ν . At rapid growth of small clusters the last two contributions in eq 10 can be neglected, and the growth law takes the form²⁸

$$n(t, t_c) \simeq n^* + c_g \rho_{cl} \mathcal{G}_{cl}^{3\nu} (t - t_c)^{3\nu} \quad (11)$$

where ν is positive.

■ COMPUTATIONAL DETAILS

Molecular dynamics simulations were performed in the spirit of previous studies of the structural transformations in this system described in refs 14 and 15 with the only difference being in the details related to the considered thermodynamic range. We have examined the system composed of $N = 8000$ particles (molecules) interacting via the mW-potential in the cubic cell with periodic boundary conditions in all directions. The time-step for numerical integration was 1 fs, and the NpT (number, pressure, temperature) ensemble was applied with $p = 1$ atm. Pressure and temperature were controlled via a Nosé–Hoover

barostat and thermostat, respectively, acting uniformly throughout the system. The damping thermostat and barostat constants were taken to be $\tau_T = \tau_P = 10$ fs. The parameters of the mW-potential are completely identical to those reported in refs 14 and 15.

Initially, the set of a hundred independent samples was prepared and equilibrated at the temperature $T = 900$ K on the time scale 50 ps (i.e., 50 000 time-steps). The correspondence of the systems to the vapor phase was directly confirmed by the particle diffusivity and the distinctive particle radial distribution functions. Moreover, following ref 15, the samples were cooled at 10 K/ns to the desired temperatures from the range $273 \leq T/K \leq 373$ (at $p \simeq 1$ atm). [It is necessary to note that the mW model reproduces correctly the equation of state $\rho(T)$ for this temperature range (see Figure 4 in ref 14).] Then, over a time scale ~ 1 – 10 ps each a system was “equilibrated” until the disappearance of the pronounced fluctuations in temperature and pressure, after that the initial configurations were stored for the further study of the vapor-to-liquid nucleation process. Note that this cooling procedure is similar to the reported one in ref 10. The following NpT simulations starting from these configurations, a hundred for each considered temperature, were performed to collect the statistics of the independent nucleated events, where the time-dependent cluster size distributions $N_n(t)$ were evaluated (for every run). The averaged time scale for the simulations in this nucleation–growth regime was 50 ns. On the basis of the found $N_n(t)$ distributions, the MFPT curves were extracted and the nucleation characteristics were estimated according to the scheme presented above. After this, the critical sizes n^* defined from the MFPT curves were used at the retreatment of the simulation data with the aim to define the distributions of the energy ω over the reaction coordinate λ .

An identification of the particles, which belong to the liquid phase, was performed in the spirit of the Stillinger rule.²⁹ First, the particles are “neighbors” (or bonded) if the distance between their centers is less than r_s , where r_s is the position of the first minimum in the pair correlation function of the liquid phase (at the same conditions). Further, a particle is considered as liquid-like if it has at least four neighbors. [The last condition allows one to remove from the consideration those particle-pairs, which are result of the instant random event and are not related to the formation of a new phase.]

RESULTS

In Figure 2 the obtained MFPT distributions τ_n^{MFPT} and their derivatives $\partial \tau_n^{\text{MFPT}} / \partial n$ at the temperatures $T = 273$, 293, and 333 K are presented as an example. On the basis of the defined values of the critical size n^* and nucleation rate $J_s = (\tau_n^{\text{MFPT}})^{-1}$, the values of the Zeldovich factor were extracted within eq 8. The typical λ dependences of the surface energy and its derivative as obtained from a single run are shown in the inset of Figure 3b. The averages of the slope $\langle d\omega/d\lambda \rangle_\lambda$ over different runs were used to estimate eq 2 by means of the trapezoidal method. The smooth character of the curves allows one to restrict oneself by the method and to exclude higher order integration schemes.³⁰ It is necessary to note that errors in the critical size n^* have not been considered at the estimation of the surface tension with eq 2.

Coordination Number. The inset of Figure 3a shows the distribution of the first coordination number for the water molecules generated by a droplet of critical size in the system at the temperature $T = 293$ K. The presented histogram is the

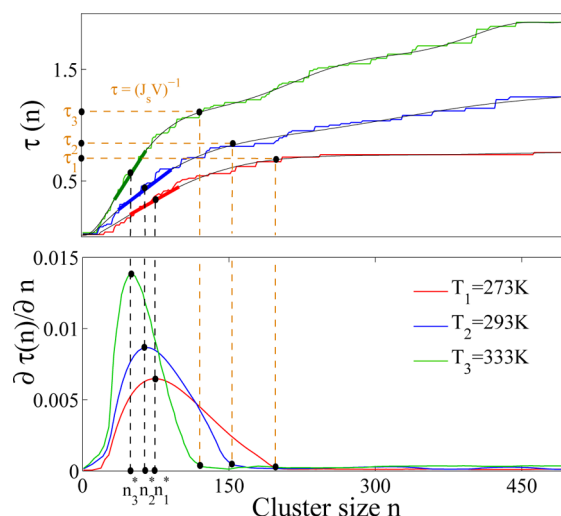


Figure 2. Top: Direct MFPT distributions (stepwise curves) and their interpolations (smooth solid curves) for the temperatures $T = 273$, 293, and 333 K. Dots on the curves indicate the inflection points, which define the critical sizes n^* , and the time scales $\tau = (J_s V)^{-1}$ corresponding to the nucleation rates. Thick short lines are the linear parts of the interpolated curves near n^* and define the ranges of errors in critical sizes. Note that the errors in the nucleation rates can be also defined as a result of changes in $\tau = (J_s V)^{-1}$ due to the correction of different interpolations with the same accuracy in the reproduction of the direct MFPT distributions. Bottom: First derivative of the MFPT distributions, $\partial \tau_n^{\text{MFPT}} / \partial n$, for the same temperatures.

cumulative result of the distributions for surface and bulk molecules. Remarkably, these distributions (for bulk and surface molecules) are symmetric ones as well as reproducible by the Gaussian functions. Further, the averaged values of the coordination numbers z and z' are extracted from the distributions and appear to be 5.8 and 3.93, respectively, for this case. Another important observation is that the term z is practically unchangeable with temperature, whereas the coordination number in a surface layer demonstrates a smooth insignificant decrease with the temperature increasing [for comparison, from $z'(T = 293\text{K}) = 3.93$ to $z'(T = 353\text{K}) = 3.47$].

Moreover, the value of the coordination number for bulk molecules in the droplets coincides with the found value of z extracted on the basis of the integral definition³¹

$$z = 4\pi\rho_l \int_0^{r_c} r^2 g(r) dr \quad (12)$$

where r_c is the first minimum position in the radial distribution function $g(r)$. Nevertheless, the found value $z(T = 293\text{K}) = 5.8$ differs from the result of Molinero and Moore¹⁴ obtained within the mW model for the bulk water, $z(T = 298\text{K}) = 5.1$. To understand the reasons for the discrepancy, we compare the corresponding radial distribution functions in Figure 3a. As can be seen, the intensity of the first maximum of $g(r)$ is higher for the case of the water droplets, although the maximum is located at a lower distance. This feature indicates that the liquid phase is characterized by the more pronounced short-range ordering for the case of the microscopically small nucleated clusters than for the equilibrium liquid phase considered in ref 14.

Surface Tension. In Figure 3b, the temperature dependence of the surface tension of the critically sized nuclei is presented. The results obtained from simulation data demonstrate the known decrease of the surface tension with

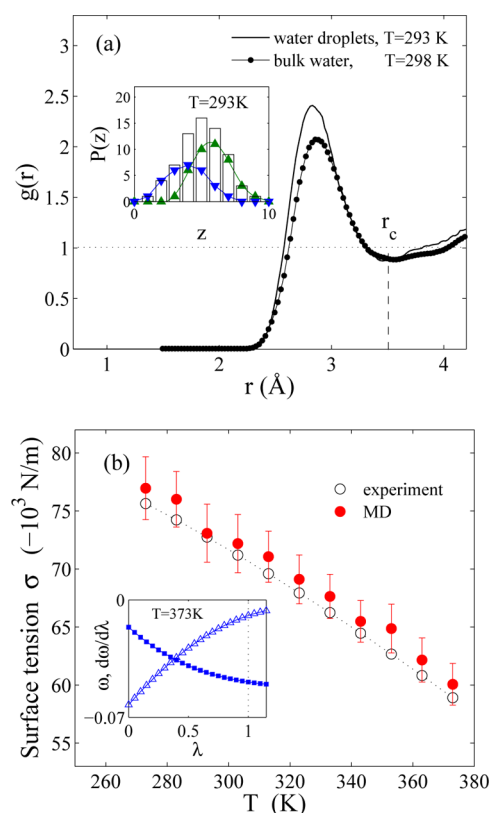


Figure 3. (a) Radial distribution function $g(r)$ of liquid water as resulted from the mW model: results for bulk water at $T = 298$ K and $p = 0$ (full circles) reported in ref 14, data for the bulk range of critically sized droplets at $T = 293$ K and $p = 1$ atm. Inset: Distribution of the first coordination number for the water molecules of a critically sized liquid droplet at the temperature $T = 293$ K. The histogram corresponds to the total distribution; the line with triangles present an impact from the bulk molecules, z ; and the line with rotated triangles shows the contribution of the surface molecules, z' . The data are averaged over a set of runs. (b) Temperature dependence of the surface tension σ . The simulation results show the averages (full circles) and standard deviations (error bars) from independent runs; experimental data are presented by open circles, whereas the dotted line is the interpolation by $\sigma(T) = B[(T_c - T)/T_c]^m \{1 + b[(T_c - T)/T_c]\}$, $B = 235.6$ N/m, $b = -0.625$, $m = 1.256$, and $T_c = 647.15$ K.³² Inset: Surface energy and slope of the surface energy $\partial\omega/\partial\lambda$ as functions of $\lambda = (N/N_c)^{1/3}$ for a growing water droplet. At the critical size $N = N_c$ one has $\lambda = 1$. The presented results are the outcome of a single simulation run.

temperature and reproduce precisely the experimental data of this term for a planar liquid–vapor interface.³² [According to results of ref 14 obtained for the planar surface tension at a single temperature $T = 300$ K, the mW model gives the best agreement with the experiment in comparison to the models: SPC, SPC/E, TIP3P, TIP4P, and TIP5P.] Such a good agreement of our results with experimental data is unexpected because of the two next reasons, mainly. First, in contrast to an inherent water system, the mW model excludes the long-range intermolecular interactions, which still can have an influence on the interface effects. Second, no adjustment of simulation data was performed to take into account the finite size effects. Thereby, the corrections to surface free energy in the spirit of the Tolman's *ansatz*, which appeared to be proportional to the inverse linear size of the critical nucleus, were unconsidered for the surface tension.

On the other hand, the surface tension of a planar interface was recently defined with the mW model for the temperatures $250 \leq T/K \leq 350$.³³ The values of the surface tension reported in ref 33 have the lower values in comparison with the values presented in Figure 3b for the water droplets, and the difference is about 5–10% for the same temperature range. Although this difference could be attributed to the Tolman length with the negative value, like it was reported by Kiselev and Ely³⁴ for the liquid–ice surface tension, we assume that our values of σ can be overestimated because of the neglect the three-particle interactions by computational protocol within eq 1.

Nevertheless, the surface tension decrease with the temperature is directly consistent with the temperature decreasing of $u(\hat{r}_{ij})$, of the surface coordination number [or the increase of the difference $(z - z')$] and of the surface particle density, where the last two contributions are practically counterbalanced by each other. [Assuming the spherical droplet of the radius R with the thickness of the surface layer Δ , the surface particle density can be roughly estimated $n'(R) \propto [R - (R - \Delta)^3/R^2]$.]

Recalling the previous debates,³⁵ the temperature range investigated here can contain the inflection points in the vapor–liquid surface tension of water. The results, presented in Figure 3b, indicate the absence of the clear detected inflections in the T -dependence of the surface tension.

Steady-State Nucleation Rate. In Figure 4, the steady-state nucleation rates obtained from the MFPT treatment of

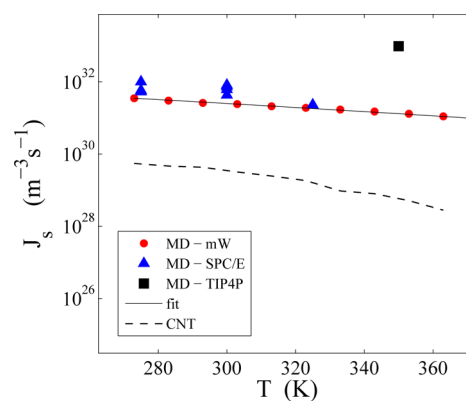


Figure 4. Temperature dependence of the homogeneous droplet (vapor-to-liquid) nucleation rate $J_s(p \approx 1 \text{ atm}, T)$ in water. Comparison of the simulation results with the mW model [the vapor density is $\rho_v \in [1.12; 1.55] \times 10^{-2} \text{ nm}^{-3}$], with the atomistic SPC/E model from ref 10 [the density is $\rho_v \in [1.23; 1.86] \times 10^{-2} \text{ nm}^{-3}$], with the atomistic TIP4P model from ref 11 [the numerical density is $\rho_v = 1.55 \times 10^{-2} \text{ nm}^{-3}$] and the treatment of nucleation data within the CNT. Solid line show the best fit by means of the function $J_s(p \approx 1 \text{ atm}, T) \propto \exp(-0.00092T^{1.4})$.

the simulation data with the mW model are presented as a function of temperature (see also Table 1). The presented data cover the density range ρ_v from $1.14 \times 10^{-2} \text{ nm}^{-3}$ to $1.55 \times 10^{-2} \text{ nm}^{-3}$. As can be seen, the values of $J_s(T)$ compare well with those obtained for the same density range by Matsubara et al. with the atomistic SPC/E model.¹⁰ Nevertheless, as contrasted to results of ref.¹⁰ which are scattered over (J_s, T) -plot, the values of the nucleation rate J_s obtained within the mW model demonstrate the smooth decrease with temperature over the considered temperature range. Moreover, this decrease is well-reproduced by the dependence $\ln[J_s(T)] = -0.00092T^{1.4} + 75$. Among all of the data presented on Figure

Table 1. Nucleation Characteristics Simulation Results: System Temperature T (K), Vapor Number Density ρ_v ($\times 10^{-2} \text{ nm}^{-3}$), Critical Cluster Size n^* , Nucleation Barrier $\Delta G/k_B$, Nucleation Rate J_s ($\times 10^{32} \text{ m}^{-3} \text{ s}^{-1}$), and the Zeldovich Factor Z

T	ρ_v	n^*	$\Delta G/k_B T$	J_s	Z
273	1.548 ± 0.095	75 ± 25	9.72 ± 2.55	0.35	0.0135 ± 0.0009
283	1.462 ± 0.060	71 ± 27	9.76 ± 2.06	0.30	0.0143 ± 0.0008
293	1.426 ± 0.077	65 ± 27	9.78 ± 2.39	0.26	0.0157 ± 0.0008
303	1.425 ± 0.051	58 ± 22	10.07 ± 1.57	0.24	0.0182 ± 0.0007
313	1.353 ± 0.062	55 ± 21	10.21 ± 2.25	0.21	0.0189 ± 0.0009
323	1.313 ± 0.047	52 ± 18	10.43 ± 2.18	0.19	0.0202 ± 0.0008
333	1.250 ± 0.037	50 ± 15	10.98 ± 2.53	0.17	0.0216 ± 0.001
343	1.224 ± 0.032	45 ± 13	11.10 ± 1.70	0.15	0.0241 ± 0.0007
353	1.174 ± 0.045	42 ± 12	11.50 ± 1.94	0.13	0.0262 ± 0.0009
363	1.140 ± 0.033	41 ± 12	11.97 ± 2.17	0.11	0.0275 ± 0.001

4a, the highest value of the nucleation rate appears from the simulations of ref 11 with the TIP4P model.

On the other hand, it is attractive to test the dependence $J_s(T)$ within the CNT treatment with the extracted values of the other nucleation characteristics. So, the original Becker–Döring formulation yields

$$J_s^{\text{CNT}} = \frac{\rho_v^2}{\rho_l} \sqrt{\frac{2\sigma_\infty}{\pi m}} \exp\left(-\frac{\Delta G_{n^*}}{k_B T}\right) \quad (13)$$

where the barrier can be taken as

$$\frac{\Delta G_{n^*}}{k_B T} = 3\pi(n^*Z)^2 \quad (14)$$

and σ_∞ is the surface tension for a planar liquid–vapor interface.³² As can be seen from Figure 4, although both dependencies demonstrate a similar behavior decaying with temperature, the pure simulation results for nucleation rate have in two orders higher values in comparison with J_s^{CNT} . This is evidence of the difficulties at the description of the droplet nucleation in water by means of the CNT, which are similar with those reported earlier for the studies with the atomistic models^{10,13} as well as with the experimental data (see Figure 3 of ref 36).

Critical Cluster (Droplet) Size. Figure 5 illustrates the temperature dependence of the critical cluster size n^* , where the simulation results with the mW model are compared with the simulation data of Matsubara et al.¹⁰ and of Yasuoka et al.¹¹ as well as with the predictions of the Kelvin equation

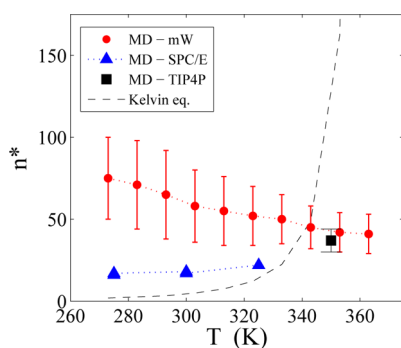


Figure 5. Temperature dependence of the critical cluster size, determined from simulations within different models of potential fields (mW model, SPC/E,¹⁰ and TIP4P¹¹), compared to predictions by the Kelvin equation. In the case of the mW model, error bars are defined by a width of the curvature range in MFPT distributions.

$$n^* = \frac{32\pi}{3} \frac{\sigma_\infty^3}{\rho_l^2 [k_B T \ln(p/p^s)]^3} \quad (15)$$

Here p^s is the saturated water vapor pressure.³⁷

First, for the mW model the critical cluster size reveals a slight decrease with temperature from $n^* = 75$ to 40 particles over the temperature range $273 \leq T/\text{K} \leq 363$. This change of the cluster size means a decrease of the droplet radius from 4 to 3.3 of the averaged water molecule diameters. Obviously, the change is insignificant. Moreover, the observed decrease is masked by errors, which were defined as the curvature range width in the MFPT distributions (see Figure 2). The range of errors is $\pm(10 \div 25)$ particles, that is determined to be reasonable, since it covers only a few surface parts of a water droplet (Figure 6). In addition, according to the definition

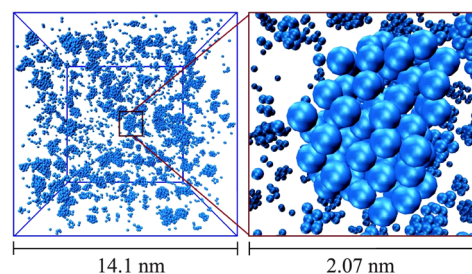


Figure 6. Left: Snapshot of the water system at the temperature $T = 293 \text{ K}$ and the pressure $p = 1 \text{ atm}$ at the moment, when the critically sized droplets are appearing. Right: Growing droplet of the same system.

within the MFPT method these errors should be considered as the probable deviations from n^* in a statistical sense. The comparison with the results obtained for the atomistic models (TIP4P and SPC/E) reveals that the values of n^* obtained within the mW model overestimate the data of the SPC/E model, but are in agreement with a single value found by Yasuoka et al. in simulations with the TIP4P model.

Further, the mW model result for the $n^*(T)$ curve is different from the predictions of eq 15, which yields an increase of n^* with the temperature T (see Figure 5). [The evaluation of the supersaturation $S = p_v/p_v^s$ was performed with the experimental values of the saturated water vapor pressure p_v^s . Nevertheless, one needs to note that the mW model can yields the results different from the experimental data for $p_v^s(T)$.] However, it should be noted that, as far as the predictions of the Kelvin equation are concerned, it gives the values $n \approx 2 \div 12$ molecules for the temperature range $273 \leq T/\text{K} \leq 363$ and the pressure p

= 1 atm. In terms of the linear cluster sizes, these values correspond to 1÷2 water molecule diameters. It is clear that the treatment of the stability of such a small cluster from the thermodynamic point of view, which requires the availability of the separated surface and bulk regions of the cluster, is impossible. [We note that the direct comparison of the predictions of the Kelvin equation with simulation results should be considered as very approximate, since the saturation curve resulted from a considered model can be different from the real water saturation curve.¹³ For the mW model, additional studies are necessary to clarify this point.]

Nucleation Barrier and the Zeldovich Factor. The temperature dependence of the next nucleation characteristic, the Zeldovich factor Z , is presented in Figure 7. As can be seen,

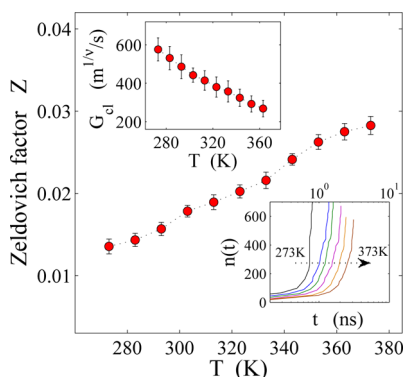


Figure 7. Main: Temperature dependence of the Zeldovich factor Z as defined by the MFPT method on the basis of the simulations with the mW model. Top inset: Temperature dependence of the growth factor G_d , which is found from the fit of eq 11 to the simulation data. The growth exponent $\nu = 1.3$ and the term $A = c_g \rho_1 (G_d t_c)^{3\nu} / n^*$ appear to be invariant with respect to the temperature. Error bars show the standard deviations from the averages. Bottom inset: Growth curves of the liquid water droplets emerging in the vapor phase at the temperatures $273 \leq T/\text{K} \leq 373$.

this quantity decreases from the value 0.028 to 0.014 with the decrease of the temperature T (see also Table 1). Such a behavior is direct evidence that the nucleation barrier loses its sharpness and becomes smoother with the decreasing the temperature. This is qualitatively in an agreement with the prediction of the CNT.²⁷ Moreover, if one assumes that the CNT yields the correct results for the vapor-to-liquid nucleation of water, then it is possible to define the nucleation barrier by means of the simple relation 14. The direct evaluation yields the correct tendency of the temperature dependence for the nucleation barrier, though this tendency is not so pronounced one as it could be expected for a sufficiently wide temperature range considered here. According to the CNT, the nucleation driving force $|\Delta\mu|$, growing with the decrease of T , must reduce the nucleation barrier.²⁷

Within eq 14 and simulation results one has that the nucleation barrier decreases from $\beta\Delta G_n^{\text{MD}} = 12 \pm 2.7$ to $\beta\Delta G_n^{\text{MD}} = 9.7 \pm 2.5$ with the decrease of the temperature from $T = 363$ to 273 K. On the other hand, the temperature dependence of the nucleation barrier as predicted by the CNT is defined by

$$\Delta G_n^* \propto \frac{\sigma_\infty^3}{\rho_1^2 |\Delta\mu|^2}$$

where $|\Delta\mu|$ is the chemical potential difference of particles in the vapor and in the liquid phase. So, the observed behavior of the nucleation barrier can be explained for the case, where the change of $\sigma_\infty^3 \rho_1^2$ with the temperature is completely counterbalanced by the change of $|\Delta\mu|^3$.

Remarkably, the comparable values for the nucleation barrier arise with the atomistic SPC/E model (see Table 1 in ref 10), where the barrier changes from $\beta\Delta G_n^* = 8.1$ to 6.7 with the temperature decreasing from $T = 325$ to 275 K. Thus, the observed results for the nucleation barrier can not be considered as a consequence of the coarse-grained character of particle interactions in the mW model.

Growth Laws of the Nucleated Droplets. The bottom inset of Figure 7 shows the growth curves of the liquid droplet at different temperatures, which were found from the statistical treatment of simulation data by means of the MFPT approach as it was discussed above. Hence, these curves depict the most probable growth laws in a statistical sense. As can be seen from the figure, at the lower temperature the droplet growth occurs faster. At the same time, all of the curves are well reproduced by eq 11, and the fitting to the simulation data yields the following features. The growth exponent ν in eq 11 appears to be invariant over the temperature T and it takes the value $\nu = 1.3$ at all of the considered temperatures. This indicates that the increase in the linear size, i.e., the radius, averaged over all of the directions of the liquid droplet follows for all of the temperatures the growth law $R(t) = (G_d t)^{1.3}$; herewith, the droplet growth itself is unsteady.

Further, the growth factor G_d decreases with the increase of the temperature T (see top inset of Figure 7), that characterizes the faster droplet growth at the lower temperatures. Following ref 28 eq 11 can be written in the rescaled form:

$$n(\xi)/n^* \simeq 1 + A(\xi - 1)^{3\nu} \quad (16)$$

where $A = c_g \rho_1 (G_d t_c)^{3\nu} / n^*$ and $\xi = t/t_c$ is the rescaled time. We found that in accordance with the rescaled form 16 all the growth curves collapse onto a single curve independently of the temperature. In addition, the parameter A in eq 16 takes the same value for all the considered temperatures, i.e., $A = 1.16 \pm 0.2$. This can be evidence of the generic features of the water droplet growth process. Remarkably, this result is correlated with the features of the crystal growth kinetics for a model glassy system under shear drive, which were reported in ref 28.

Shape and Sphericity of the Nucleated Droplets. Other issue, which is crucial in the CNT, is related with the shape and the anisotropy of the growing droplets.^{16,38} A convenient way to perform this study in our case is to use the asphericity parameter in the next definition:

$$S_0 = \left\langle \frac{(I_{xx} - I_{yy})^2 + (I_{xx} - I_{zz})^2 + (I_{yy} - I_{zz})^2}{2(I_{xx} + I_{yy} + I_{zz})^2} \right\rangle$$

where

$$I_{\alpha\beta} = \sum_{i=1}^{n^*} m_0 (r_i^2 \delta_{\alpha\beta} - r_{i\alpha} r_{i\beta})$$

is the components of the moment of inertia tensor associated with a droplet, m_0 is the molecule mass, $\alpha, \beta \in \{x, y, z\}$ are the components of the vector \vec{r} between the droplet center-of-mass and molecule i ; the brackets $\langle \dots \rangle$ mean the statistical average over critically sized droplets of the different simulation runs.

This definition of a sphericity parameter sets the characterization: for a spherical droplet one has $S_0 = 0$, whereas for an elongated and string-like cluster one obtains $S_0 \rightarrow 1$. We found that independently on the particular conditions (temperature, vapor density) the asphericity parameter for the considered (p, T) range is $S_0 \simeq 0.008 \pm 0.0002$. It indicates on the nucleated water droplets of the sphere-like form, which is also confirmed by a visual inspection of snapshots (Figure 6). We remark here, this result is not the same as the findings of refs 10 and 11, where the detected critical clusters in water had the significant deviations from a spherical form. A possible reason affecting the observed discrepancy could be different cluster definitions applied by Matsubara et al. in ref 10 and used in the present study within the statistical treatment. In addition, the low values for the nucleated droplets were obtained in ref 10, $n^* \simeq 16 \div 22$ particles, and the pronounced deviation from a spherical form can be considered as a signature of the finite size effects: a weak structural rearrangement in such a system raises the significant change of its shape.

CONCLUSIONS

The coarse-grained models for particle interactions in molecular systems provide a good opportunity to study early stages of the phase transitions by means of numerical simulations. In this work, the processes of the steady-state homogeneous vapor-to-liquid nucleation and the growth of liquid droplets in water were considered within the mW model, which treats the molecular interactions excluding any details of the direct oxygen–hydrogen interactions and electrostatics. Despite the apparent coarsening in the description of the molecular interactions, we have shown that the mW model provides interesting information concerning the droplet nucleation in water vapor, thereby complementing the simulation results obtained earlier within all-atom models of water such as TIP4P and SPC/E.^{10,11,31,39} It is necessary to note that the results reported here are obtained on the basis of the extended statistical treatment within the MFPT approach and the thermodynamic integration scheme.

The surface tension of the nucleated droplets was computed within an approximation that is restricted by the consideration of the two-particle interactions only without handling the three-particle contribution to the energy of system. The obtained values demonstrate the decrease of the surface tension with the temperature growth. It is necessary to note that the applied numerical scheme gives higher values for the liquid–vapor surface tension of the droplets in comparison with the values for the liquid–vacuum surface tension of a planar interface reported in ref 14 and 33. We suppose that this difference is a result of the approximations applied to the surface tension definition rather than the mW model product.

Further, the evaluated values of the steady-state nucleation rate are comparable with the results for all-atom models as well as with the treatments within the classical nucleation theory. Unfortunately, we could not to perform a direct comparison of the obtained nucleation rates with the experimental data, because we found no experimental J_s for the (p, T) line considered here. Nevertheless, quantitative extrapolation of the obtained outcomes indicates on the difference between simulated and experimental results, that is similar with the known difference between the experimental data and the CNT predictions.^{9,40} On the other hand, for the critical size of the nucleated droplet, we found the values within the range $30 \div 100$ particles, which are expected to be comparable with the

experimental data (Figure 13 in ref 9). So, the additional studies are highly desirable in this field.

According to our results, the growth of nucleated droplets in the system is characterized by remarkable features: the growth law of the droplet radius follows the power law, $R(t) \propto t^{1/3}$, and the growth is not steady (with the time-dependent growth rate $G(t) \propto t^{0.3}$). Moreover, the simple rescaling on the critical droplet characteristics yields the unified form of the growth law at all of the considered temperatures.

Finally, we found that the critically sized droplets have a shape, which is close to spherical one. Note that the deviations from spherical shape of the water droplets at homogeneous nucleation, which were established for the SPC/E model by Matsubara et al. (see ref 10), could be simply originated from the extremely low obtained values for the critical size n^* .

AUTHOR INFORMATION

Corresponding Author

*E-mail: anatolii.mokshin@mail.ru.

Notes

The authors declare no competing financial interest.

ACKNOWLEDGMENTS

The authors acknowledge B. N. Hale for helpful correspondence and R. M. Khusnutdinoff for many useful discussions.

REFERENCES

- (1) Wölk, J.; Strey, R. *J. Phys. Chem. B* **2001**, *105*, 11683–11701.
- (2) Kim, Y. J.; Wyslouzil, B. E.; Wilemski, G.; Wölk, J.; Strey, R. *J. Phys. Chem. A* **2004**, *108*, 4365–4377.
- (3) Manka, A. A.; Brus, D.; Hyvärinen, A. -P.; Lihavainen, H.; Wölk, J.; Strey, R. *J. Chem. Phys.* **2010**, *132*, 244505 1–10.
- (4) Brus, D.; Ždimal, V.; Uchtmann, H. *J. Chem. Phys.* **2009**, *131*, 074507 1–9.
- (5) Brus, D.; Ždimal, V.; Smolík, J. *J. Chem. Phys.* **2008**, *129*, 174501 1–8.
- (6) Mikheev, V. B.; Irving, P. M.; Laulainen, N. S.; Barlow, S. E.; Pervukhin, V. V. *J. Chem. Phys.* **2002**, *116*, 10772–10786.
- (7) Luijten, C. C. M.; Bosschaart, K. J.; van Dongen, M. E. H. *J. Chem. Phys.* **1997**, *106*, 8116–8123.
- (8) Heist, R. H.; He, H. *J. Phys. Chem. Ref. Data* **1994**, *23*, 781–804.
- (9) Viisanen, Y.; Strey, R.; Reiss, H. *J. Chem. Phys.* **1993**, *99*, 4680–4692.
- (10) Matsubara, H.; Koishi, T.; Ebisuzaki, T. *J. Chem. Phys.* **2007**, *127*, 214507 1–11.
- (11) Yasuoka, K.; Matsumoto, M. *J. Chem. Phys.* **1998**, *109*, 8451–8462.
- (12) Merikanto, J.; Vehkamäki, H.; Zapadinsky, E. *J. Chem. Phys.* **2004**, *121*, 914 1–24.
- (13) Chen, B.; Siepmann, J. I.; Klein, M. L. *J. Phys. Chem. A* **2005**, *109*, 1137–1145.
- (14) Molinero, V.; Moore, E. B. *J. Phys. Chem. B* **2009**, *113*, 4008–4016.
- (15) Moore, E. B.; Molinero, V. *Nature* **2011**, *479*, 506–508.
- (16) Reinhardt, A.; Doye, J. P. K. *J. Chem. Phys.* **2012**, *136*, 054501 1–11.
- (17) Bartell, L. S.; Turner, G. W. *J. Phys. Chem. B* **2004**, *108*, 19742–19747.
- (18) Mokshin, A. V.; Yulmetyev, R. M.; Khusnutdinoff, R. M.; Hanggi, P. *J. Phys.: Condensed Mater.* **2007**, *19*, 046209 1–16.
- (19) Berry, M. V.; Durrans, R. F.; Evans, R. J. *Phys. A: Gen. Phys.* **1972**, *5*, 166–70.
- (20) Horsch, M.; Hasse, H.; Shchekin, A. K.; Agarwal, A.; Eckelsbach, S.; Vrabec, J.; Müller, E. A.; Jackson, G. *Phys. Rev. E* **2012**, *85*, 0316051–12.

- (21) Wedekind, J.; Strey, R.; Reguera, D. *J. Chem. Phys.* **2007**, *126*, 134103 1–7.
- (22) Mokshin, A. V.; Barrat, J.-L. *Phys. Rev. E* **2008**, *77*, 0215051–7.
- (23) Mokshin, A. V.; Barrat, J.-L. *J. Chem. Phys.* **2009**, *130*, 034502 1–6.
- (24) Frenkel, J. *Kinetic Theory of Liquids*; Oxford University Press: London, 1946.
- (25) Hansen, J. P.; McDonald, I. R. *Theory of Simple Liquids*; Academic Press: New York, 2006.
- (26) Hänggi, P.; Talkner, P.; Borkovec, M. *Rev. Mod. Phys.* **1990**, *62*, 251–342.
- (27) Kashchiev, D. *Nucleation: Basic Theory with Applications*; Butterworth Heinemann: Oxford, U.K., 2000.
- (28) Mokshin, A. V.; Barrat, J.-L. *Phys. Rev. E* **2010**, *82*, 0215051–9.
- (29) Stillinger, F. H. *J. Chem. Phys.* **1963**, *38*, 1486–1494.
- (30) Ytreberg, F. M.; Swendsen, R. H.; Zuckerman, D. M. *J. Chem. Phys.* **2006**, *125*, 184114 1–11.
- (31) Khusnutdinoff, R. M.; Mokshin, A. V. *Physica A* **2012**, *391*, 2842–2847.
- (32) IAPWS Release on Surface Tension of Ordinary Water Substance, IAPWS, 1994 (<http://www.iapws.org/relguide/surf.pdf>).
- (33) Baron, R.; Molinero, V. *J. Chem. Theory Comput* **2012**, in press, (DOI: 10.1021/ct300121r).
- (34) Kiselev, S. B.; Ely, J. F. *Physica A* **2001**, *299*, 357–370.
- (35) Lü, Y. J.; Wei, B. *Appl. Phys. Lett.* **2006**, *89*, 1641061–3 and references therein..
- (36) Hale, B. N. *J. Chem. Phys.* **2005**, *122*, 204509 1–3.
- (37) Alexandrov, A. A.; Grigoriev, B. A. *Tables of Thermophysical Properties of Water and Steam*; MEI: Moscow, Russia, 1999.
- (38) Rodney, D.; Tanguy, A.; Vandembroucq, D. *Modell. Simul. Mater. Sci. Eng.* **2011**, *19*, 0830011–49.
- (39) Khusnutdinoff, R. M.; Mokshin, A. V. *J. Non-Cryst. Solids* **2011**, *357*, 1677–1684.
- (40) Hale, B. N.; Thomason, M. *Phys. Rev. Lett.* **2010**, *105*, 046101 1–4.